Millimeter-Wave Device-to-Device Networks with Heterogeneous Antenna Arrays

Na Deng, *Member, IEEE*, Martin Haenggi, *Fellow, IEEE*, and Yi Sun, *Member, IEEE*

***Abstract*—Millimeter-wave (mm-wave) device-to-device (D2D) communication is considered one of the most promising enabling technologies to meet the demanding requirements of future networks. Previous works on mm-wave D2D network analysis mostly considered the case that all devices were equipped with exactly the same number of antennas, whereas real networks are more complicated due to the coexistence of diverse devices. In this paper, we present a comprehensive investigation on the interference characteristics and link performance in mm-wave D2D networks where the concurrent transmission beams are varying in width. First, we establish a general and tractable framework for the target network with Nakagami fading and directional beamforming. To fully characterize the interference, we derive the mean and variance of the interference and then provide an approximation of the interference distribution by a mixture of the inverse gamma and the log-normal distributions. More importantly, the coexistence of varied beamwidths renders their interactions and thus the interference quite complicated and sensitive to the antenna pattern, highlighting the significance of adopting an accurate model for the antenna pattern. Second, to show the impact of heterogeneous antenna arrays on the link performance, we derive the signal-to-interference-plus-noise ratio (SINR) and rate distributions of the typical receiver as well as their asymptotics, bounds, and approximations to get deep insights on the performance of the network.**

***Index Terms*—Stochastic geometry; Poisson point process; millimeter wave; D2D communication; interference distribution; success probability; rate distribution.**

I. Introduction

A. Motivation

The proliferation of high-speed multi-media applications and high-end devices (e.g., smartphones, laptops, machine-to-machine communication devices, etc.) exacerbates the demand for high data rate services. According to the latest visual network index (VNI) report from Cisco [2], the global mobile data traffic will increase nearly sevenfold between 2016 and 2021, reaching 49.0 exabytes per month by 2021, wherein more than three-fourths will be video. The need for greater capacity, and hence greater spectrum utilization, has very recently led to the advent of device-to-device (D2D) communications in the millimeter wave (mm-wave) band to efficiently use the large bandwidth (multiple gigahertz).

Millimeter wave communication and networking is concerned with taking advantage of the vast amount of spectrum available in the range of 30 to 300 GHz, which offers great potential in achieving the 100x data rate increase. Moreover, the very short wavelength makes it possible to adopt relatively large antenna arrays in mobile terminals. Unlike the conventional sub-6 GHz systems, mm-wave signals have been confirmed to have some unique propagation characteristics, such as the huge propagation losses and the susceptibility to blockages [3]. Thus, on the one hand, beamforming is generally employed to achieve substantial array gains and synthesize highly directional beams; on the other hand, the communication distance is relatively short, despite the beamforming.

In addition to mm-wave communication, D2D communication is another key enabler of next-generation wireless networks that has recently received widespread attention, with the goal of reducing the traffic load of base stations (BSs), increasing the spectral efficiency, and improving the quality of experience (QoE) at the cell-edge users [4–7]. From the above discussions, mm-wave and beamforming can easily be integrated with D2D communication for interference reduction and further improved spectrum utilization. However, this emerging technology is still in its infancy, and it is unclear what benefits and challenges it will bring. It is clear that mm-wave D2D communication is more complicated than sub-6 GHz D2D and mm-wave cellular communications. Firstly, the narrow beam width of mm-wave and the relatively low antenna height (compared with that of BSs) render the mm-wave D2D communication even more vulnerable to blockages. Secondly (and more importantly), different from the cellular BSs that are usually equipped with homogeneous antenna arrays (namely the same number of antennas), the devices have their inherent diverse properties and random locations, which means devices in the network cannot be expected to be equipped with the same number of antennas and located in a well-planned manner. In mm-wave networks, since the signal and interference power are closely related to the angles of departure/arrival (AoDs/AoAs) and transmission beam widths, the heterogeneity of the antenna arrays yields more complex interference environments and poses a challenge for the performance analysis. Therefore, in this paper, we will present a comprehensive investigation of the interference characteristics and link performance for heterogeneous mm-wave D2D networks and obtain useful insights for the further development of mm-wave D2D communications.

Na Deng and Yi Sun are with the School of Information and Communication Engineering, Dalian University of Technology (DLUT), Dalian, 116024, China (e-mail: dengna,lslwf@dlut.edu.cn). Martin Haenggi is with the Dept. of Electrical Engineering, University of Notre Dame, Notre Dame 46556, USA (e-mail: mhaenggi@nd.edu).

Part of this paper has been accepted at the IEEE Wireless Communications and Networking Conference in 2018 [1].

This work was supported by the National Natural Science Foundation of China under Grant 61701071, by the China Postdoctoral Science Foundation (2017M621129), by the Fundamental Research Funds for the Central Universities (DUT16RC(3)119), and by the US NSF grant CCF 1525904.

B. Related Work

Motivated by the mathematical flexibility of the Poisson point process (PPP)-based abstraction, several researchers have recently turned their attention to the study of the performance of mm-wave networks with the aid of stochastic geometry [8–13]. Because of the distinguishing features of mm-wave networks, such as the propagation environment and the use of highly directional antenna arrays at the transceivers, models for networks operating in the sub-6 GHz band are not directly applicable to analyze mm-wave networks. Thus, it is necessary to develop a mathematical framework specifically tailored to the salient features of mm-wave channels and transmission schemes.

To maintain analytical tractability, the actual beamforming patterns were usually approximated by a sectored model in earlier work, i.e., the antenna pattern was simplified as a *flat-top* pattern [9–12]. In essence, the flat-top antenna pattern quantizes the continuously varying antenna array gains in a binary manner. Although this significantly simplifies the analytical results, the oversimplified pattern leads to deviations from the actual performance [13]. The impact of this deviation was reduced to a certain extent by the assumption of homogeneous directional antenna arrays with exactly the same number of antennas and antenna model at all nodes. Without this assumption, the performance gap is even larger, as will be revealed in this paper. In fact, with the rapid development of radio access technologies, the network nodes can be expected to be diverse in terms of the number of antennas, beamwidth, and multi-antenna transmission schemes, especially for D2D networks composed of different kinds of devices. For instance, [14] proposed a hybrid antenna composed of two modules (2×2 and 8×8 MIMO configurations) for future multi-mode smartphone applications. Very recently, a multi-lobe approximation for the actual antenna pattern was proposed in [15], which is an extended version of the flat-top antenna pattern from the binary version to an M-ary quantization. Though a finer approximation is provided, the relationship between the antenna pattern and the number of antennas is not explicitly given, which means it is not possible to characterize the effect of heterogeneity of antenna arrays on the performance.

Although mm-wave devices offer several potential advantages for D2D networks, there has been limited application of stochastic geometry to study the potential performance of mm-wave D2D networks incorporating key features of the mm-wave band. The primary related works are [9] and [13]: the former approximated the directional beamforming by a sectored model with the assumption of homogeneous antenna arrays and blockage effects but considered a finite number of interferers in a finite network region; while the latter proposed two more accurate antenna pattern models with the same assumption in [9]. In contrast, our prior work in [16] used stochastic geometry to provide a fine-grained performance analysis of mm-wave D2D networks in terms of the *meta distribution*, and it also considered the simplified flat-top antenna pattern with uniform antenna array.

In summary, to the best of our knowledge, the effect of the heterogeneity of the antenna arrays on the potential performance of mm-wave D2D networks has not been studied in conjunction with accurate approximations for the actual antenna pattern. In this work, we will fill this gap with new analytical results of the interference characteristics and SINR performance in a stochastic geometry framework.

C. Contributions

The main objective of this paper is to carry out a comprehensive investigation on the impact of the node/device diversity on the interference characteristics and link performance in mm-wave D2D networks. The main contributions of this work are summarized as follows.

- We first develop a tractable model and general mathematical framework with Nakagami fading for the performance analysis in mm-wave D2D networks by using the K-tier homogeneous independent Poisson point process (HIP) model [17, Def. 2] to capture the node locations, and different tiers correspond to different kinds of devices that may differ in terms of the density, antenna array size, transmit power, etc. The blockage effect is reflected by a general LOS ball blockage model [18], and the cosine antenna pattern [13], confirmed to be an accurate as well as tractable approximation for the actual antenna pattern, is adopted.
- To show the interference characteristics in the mm-wave D2D network, we give closed-form expressions for the mean and variance of the interference. Based on the maximum likelihood estimation method, we further provide an approximation for the interference distribution by a mixture of the inverse gamma and the log-normal distributions.
- Based on the general framework, analytical expressions for the SINR and rate distributions of the mm-wave D2D network are provided. To make the analytical results more tractable for practical evaluation, two efficient approaches are taken: one is to bound the performance, and the other one is to get approximate performance results. Numerical results show the tightness of the bound and the accuracy of the approximations.
- With the highly tractable analytical results, the impacts of the distinguishing mm-wave features, the coexistence of devices with different number of antennas, and the density of devices on each performance metric are investigated numerically. The results highlight the significance of adopting an accurate model for the antenna pattern and provide useful insights on how to efficiently operate D2D communication in mm-wave bands.

D. Organization

The rest of the paper is organized as follows: Sec. II introduces the system model with antenna pattern gain and blockage effect. Sec. III derives the mean and variance of the interference and provides an approximation of the interference distribution. Sec. IV analyzes the SINR and rate distributions as well as the impact of heterogeneous antenna arrays with exact analytical results, asymptotics, bounds, and approximations, and Sec. V offers the concluding remarks.

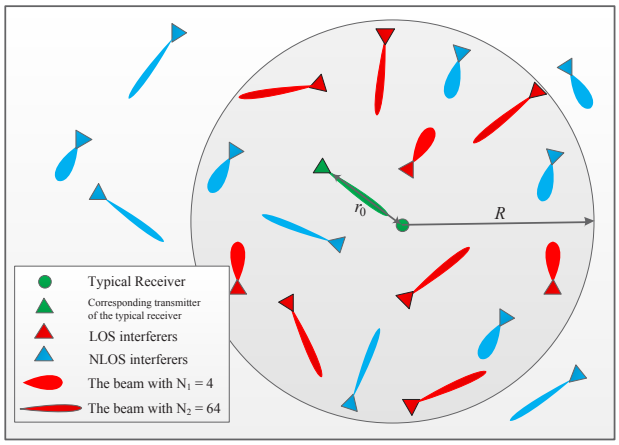

Fig. 1. A sample mm-wave D2D network where transmitters are modeled as a PPP with two types of antenna arrays, i.e., $N_1 = 4$ and $N_2 = 64$. The different beam lengths and widths correspond to the antenna gains of different array sizes.

II. System Model

A. Network Model

It is assumed that the transmitters belonging to the k-th tier are distributed uniformly in the two-dimensional Euclidean space $\mathbb{R}^2$ according to a homogeneous PPP Φ_k of density λ_k, equipped with N_k antennas and operating at a constant transmit power μ_k. For all $j \neq i$, Φ_j and Φ_i are independent. The ALOHA channel access scheme is adopted, i.e., in each time slot, D2D transmitters in Φ_k independently transmit with probability q_k. Accordingly, the distribution of the devices in mm-wave D2D networks is defined as $\Phi = \bigcup_{k=1}^{K} \Phi_k$ with density $\lambda = \sum_{k=1}^{K} \lambda_k$. Each transmitter is assumed to have a dedicated receiver at distance r_0 in a random orientation, i.e., the D2D users form a K-tier *Poisson bipolar network* [19, Def. 5.8]. Without loss of generality, we consider a receiver at the origin that attempts to receive from an additional transmitter located at $(r_0, 0)$. Due to Slivnyak's theorem [19, Thm. 8.10], this receiver becomes the typical receiver under expectation over the (overall) PPP. To analyze the typical D2D receiver belonging to the k-th tier, we further condition on that receiver at the origin to belong to the k-th tier with parameters (such as transmit power, number of antennas, etc.) chosen from that tier. Fig. 1 gives an example of a two-tier mm-wave D2D network with two types of transmitters differing in the number of transmitting antennas.

B. Directional Beamforming Model

We assume that the transmitters belonging to k-th tier are equipped with a uniform linear array (ULA) composed of N_k antenna elements to perform directional beamforming and that their corresponding receivers have a single antenna[1]. It is also assumed that the transmitter knows the direction to the receiver so that it can point its AoD at its receiver perfectly to obtain the maximum power gain. For the k-th tier, the array gain function of the actual antenna pattern is expressed as [20]

$$G_{k,\mathrm{act}}(\varphi) = \frac{\sin^2(\pi N_k \varphi)}{N_k \sin^2(\pi \varphi)}, \tag{1}$$

where $\varphi = \frac{d_\mathrm{t}}{\varrho} \cos\phi$ is the cosine direction corresponding to the AoD ϕ of the transmit signal, which is termed as the *spatial AoD*, with d_t and ϱ representing the antenna spacing and wavelength, respectively. d_t is usually set to be half-wavelength to enhance the directionality of the beam and avoid grating lobes; φ is assumed to be uniformly distributed in $[-0.5, 0.5]$, and thus the spatial AoD from an interferer to the typical receiver is also uniformly distributed in $[-0.5, 0.5]$, as proven in [13]. Although this function has a relatively simple expression, it does not lend itself to further analysis due to the sine functions in both the numerator and denominator.

Recently, an accurate approximation termed *cosine antenna pattern* was proposed in [13], which is shown to constitute a desirable trade-off between accuracy and tractability in the performance analysis of mm-wave networks. This antenna pattern approximation is based on the cosine function with the antenna gain function (for the k-th tier)

$$G_k(\varphi) = \begin{cases} N_k \cos^2\left(\frac{\pi N_k}{2}\varphi\right) & \text{if } |\varphi| \leq 1/N_k \\ 0 & \text{otherwise,} \end{cases} \tag{2}$$

For the commonly used flat-top antenna pattern, the array gains within the half-power beamwidth (HPBW) are assumed to be the maximum power gain, and the array gains corresponding to the remaining AoDs are approximated to be the first minor maximum gain of the actual antenna pattern. Thus, the antenna gain function for the k-th tier can be approximately expressed as

$$G_{k,\mathrm{flat}}(\varphi) = \begin{cases} G_{k,\mathrm{m}} & \text{if } |\varphi| \leq w_{k,\mathrm{m}} \\ G_{k,\mathrm{s}} & \text{otherwise,} \end{cases} \tag{3}$$

where $w_{k,\mathrm{m}}$ is chosen as the HPBW, i.e. $G_{k,\mathrm{act}}(w_{k,\mathrm{m}}) = N_k/2$, $G_{k,\mathrm{m}} = N_k$ and $G_{k,\mathrm{s}} = G_{k,\mathrm{act}}\left(\frac{3}{2N_k}\right)$. Although this simple approximation is highly tractable, it causes significant deviations from the actual performance, especially when there are differences in the number of antennas among different devices in the network. To cope with this inaccuracy, we further consider a *normalized flat-top antenna pattern* with the antenna gain function for the k-th tier as follows

$$G_{k,\mathrm{norm}}(\varphi) = \begin{cases} G_{k,\mathrm{m}} & \text{if } |\varphi| \leq w_{k,\mathrm{m}} \\ \frac{1-2w_{k,\mathrm{m}}G_{k,\mathrm{m}}}{1-2w_{k,\mathrm{m}}} & \text{otherwise,} \end{cases} \tag{4}$$

where the side lobe gain is modified to make the integral of antenna gain function over the range of the spatial AoD equal to 1 (as in (1)).

Next, we compare the cosine antenna pattern, the non-normalized and normalized flat-top antenna pattern, as well as the actual antenna pattern. From the actual antenna pattern, shown in Fig. 2, we can observe that the first side lobe gain of $N = 64$ is within 1 dB of the main lobe gain of $N = 4$ but restricted to quite a small range of AoDs, which means the side lobe leakage causes high interference to other devices in a very narrow range of directions. For the flat-top pattern, the array gains corresponding to all the directions

[1]We make this assumption for analytical tractability. The generalization to N_k antennas at the receiver is straightforward, by reforming the desired and interfering signals with the receiving array gains and modifying the mathematical derivation of the interference Laplace transform in Sec. IV.

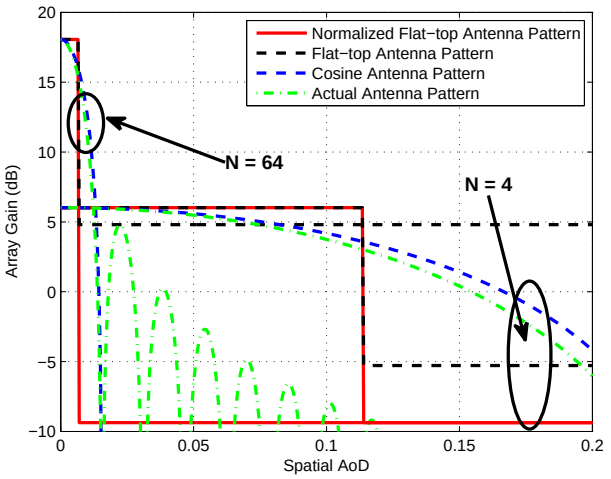

Fig. 2. Visualization of four different antenna patterns for $N = 4$ and $N = 64$.

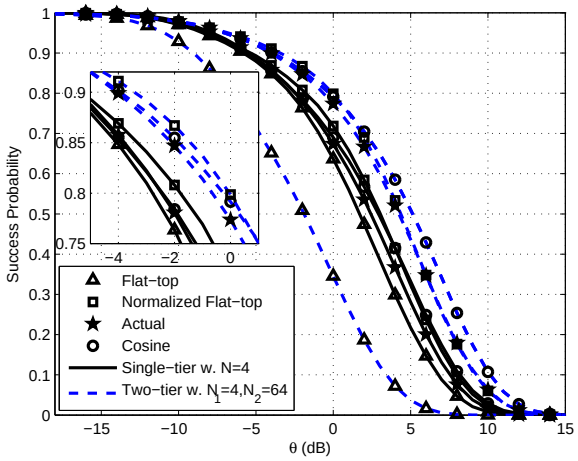

(a) Success probability for a device with 4 antennas.

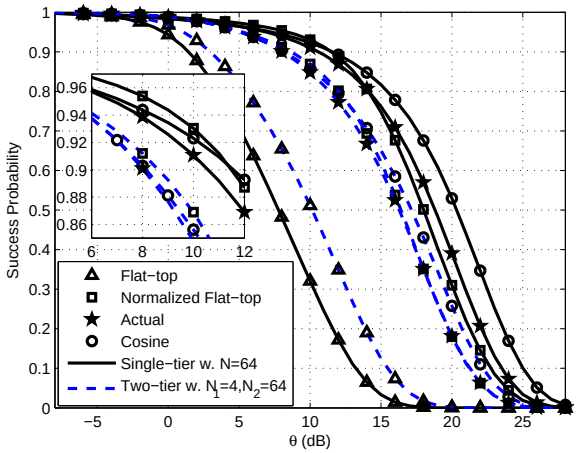

(b) Success probability for a device with 64 antennas.

Fig. 3. Comparisons of success probabilities using three different antenna patterns in single-tier and two-tier networks, respectively. The network parameters are listed in Table I.

outside the main lobe are assumed to be equal to the first side lobe gain of the actual pattern. Obviously, this approximation leads to deviation from the actual antenna pattern because it exaggerates the effect of side lobe leakage. The larger the number of antennas, the greater the deviations. It is even worse for networks where different kinds of devices are likely to be equipped with different numbers of antennas. Although the side lobe gain of the normalized flat-top antenna pattern is significantly reduced via the gain normalization, both the non-normalized and normalized flat-top antenna patterns cannot reflect the roll-off characteristics for the main lobe of the actual pattern, which, however, is perfectly approximated by the cosine antenna pattern.

To further illustrate the importance and necessity of adopting accurate approximations for the antenna pattern more visually, we also compare the four antenna patterns in terms of the link success probability $\mathbb{P}(\text{SINR} > \theta)$ in Fig. 3, where SINR is the signal-to-interference-plus-noise ratio, as defined in Sec. II-D. Specifically, Fig. 3(a) compares the performance of a device equipped with 4 antennas in a single-tier and two-tier network, respectively. The single-tier network is homogeneous, where all devices are equipped with 4 antennas, i.e., $N = 4$ and $\lambda = 0.1$; while the two-tier network is heterogeneous, where devices equipped with 4 and 64 antennas coexist in a network with the same density, i.e., $N_1 = 4$, $N_2 = 64$ and $\lambda = 0.1$ ($\lambda_1 = \lambda_2$). It is seen that both the cosine antenna pattern and the normalized antenna pattern provide good approximations of the actual performance in both networks. To be specific, the curves of cosine pattern always provide an upper bound on that of the actual one while the curves of the normalized flat-top pattern have intersection points with that of the actual one. However, for the (non-normalized) flat-top antenna pattern, due to the fatal yet faux interference caused by the unsuitable modeling of the side lobe gain, its performance approximation is obviously deviated from the actual performance and the trend of the performance change from one-tier to two-tier is even opposite to that of the other three antenna patterns. These observations demonstrate that the parameters for the flat-top pattern need to be carefully chosen in order to approximate the actual antenna pattern accurately.

In summary, both the cosine and the normalized flat-top antenna patterns provide good approximations in terms of the success probability. However, from the view of the antenna pattern itself, the flat-top antenna pattern is inferior to the cosine antenna pattern due to its binary quantization of the array gains which cannot reflect the roll-off characteristics of the main lobe well. The roll-off characteristics, in fact, is quite critical for mm-wave communications. For example, when beam misalignment is considered or when the angle of beam is slightly adjusted to cause significantly less interference at the nearby other receivers, the desired signal power may not be the maximum power gain but some smaller gain on the roll-off curve. Clearly, any flat-top pattern would be highly inaccurate in such cases, while the cosine pattern would still do quite well since its main lobe matches the actual one extremely well and its first null is at the right angle. Thus, taking both accuracy

TABLE I. Symbols and descriptions

Symbol	Description	Default value
K	The number of tiers differ in antenna array size	3
Φ_i, λ_i	The i-th tier mm-wave device PPP and density	$\mathrm{N/A}, 0.1/\mathrm{m}^2$
μ_i	The transmit power for the i-th tier device	20 dB
N_i	The number of antennas for the i-th tier device	N/A
W	mm-wave bandwidth	2GHz
r_0	The link distance between D2D users	2m
d_0	The parameter of bounded path loss law	1m
q_i	The transmit probability for the i-th tier device in each time slot	1
$p_{\mathrm{L}}/p_{\mathrm{N}}$	The probability of a link being LOS/NLOS	$0.2/0.8$
$\alpha_{i,\mathrm{L}}/\alpha_{i,\mathrm{N}}$	The path loss exponent of the LOS/NLOS link for the i-th tier device	$2.5/4$
$M_{i,\mathrm{L}}/M_{i,\mathrm{N}}$	The Nakagami parameter of the LOS/NLOS link for the i-th tier device	$4/2$
R	The radius of the generalized LOS ball	200m
θ	The SINR threshold	N/A

and tractability into consideration, the cosine antenna pattern is adopted in the following analysis, which makes it possible to investigate the impact of heterogeneous antenna arrays on the interference environment and link performance.

C. Blockage and Propagation Model

The signal path can be either LOS/unblocked or NLOS/blocked, each with a different path loss exponent. The generalized LOS ball model [18] is adopted to capture the blockage effect in mm-wave communication, which was verified to be as accurate as the empirical 3GPP blockage model by experiments in [8]. Specifically, the LOS probability of the signal path between two nodes with separation d is

$$P_{\mathrm{LOS}}(d) = p_{\mathrm{L}}\mathbf{1}(d < R), \tag{5}$$

where $\mathbf{1}(\cdot)$ is the indicator function, R is the maximum length of a LOS channel, and $p_{\mathrm{L}} \in [0,1]$ is the LOS probability if $d \leq R$. Let $\alpha_{k,\mathrm{L}}$ and $\alpha_{k,\mathrm{N}}$ denote the path loss exponents of LOS and NLOS paths belonging to the k-th tier, respectively. Typical values for mm-wave path loss exponents can be found in [21] with approximated ranges of $\alpha_{k,\mathrm{L}} \in [1.9, 2.5]$ and $\alpha_{k,\mathrm{N}} \in [2.5, 4.7]$.

D. Signal-to-interference-plus-noise Ratio (SINR)

We assume that the desired link between the transmitter-receiver pair is in the LOS condition with deterministic path loss $r_0^{-\alpha_{k,\mathrm{L}}}$ given that the typical receiver belongs to the k-th tier. In fact, if the receiver was associated with a NLOS transmitter, the link would quite likely be in outage due to the severe propagation loss and high noise power at mm-wave bands as well as the fact that the interferers can be arbitrarily close to the receiver. Different path loss exponents are applied to the cases of LOS and NLOS paths. We denote by $\ell_k(x)$ the random path loss function associated with the interfering transmitter location $x \in \Phi_k$, given by

$$\ell_k(x) = \begin{cases} (\max\{d_0, |x|\})^{-\alpha_{k,\mathrm{L}}} & \text{w.p. } P_{\mathrm{LOS}}(|x|) \\ (\max\{d_0, |x|\})^{-\alpha_{k,\mathrm{N}}} & \text{w.p. } 1-P_{\mathrm{LOS}}(|x|), \end{cases} \tag{6}$$

where all $\ell_k(x)_{x\in\Phi_k}$ are independent. In addition to the distance-dependent path loss, we assume independent Nakagami fading for each path, which is a sensible model given the LOS-dependent mm-wave scenarios. Different Nakagami fading parameters $M_{k,\mathrm{L}}$ and $M_{k,\mathrm{N}}$ are assumed for LOS and NLOS paths in the k-th tier, where $M_{k,\mathrm{L}}$ and $M_{k,\mathrm{N}}$ are positive integers. The power fading coefficient between node $x \in \Phi_k$ and the origin is denoted by h_x, which follows a gamma distribution $\mathrm{Gamma}(M, \frac{1}{M})$ with $M \in \{M_{k,\mathrm{L}}, M_{k,\mathrm{N}}\}$, and all h_x are mutually independent and also independent of the point process. For the typical receiver, the interferers outside the LOS ball are NLOS and thus can be ignored due to the severe path loss over the large distance (at least R). As a result, the analysis for the network originally composed of multiple PPPs reduces to the analysis of a finite network region, and the relevant transmitters, denoted as $\hat{\Phi}_k$, correspond to the PPP in a disk of radius R centered at the origin. Based on this model, the interference from tier k at the origin is

$$I_k = \sum\nolimits_{x\in\hat{\Phi}_k} \mu_k G_k(\varphi_x) h_x \ell_k(x) B_k(x), \tag{7}$$

where $G_k(\varphi_x)$ is the directional antenna gain function with spatial AoD φ_x following Eq. (2), and $B_k(x)$ is a Bernoulli variable with parameter q_k to indicate whether x transmits a message to its receiver. Due to the incorporation of the blockages, the LOS transmitters belonging to the k-th tier with LOS propagation to the typical receiver form a PPP $\hat{\Phi}_{k,\mathrm{L}}$ with density $p_{\mathrm{L}}\lambda_k$, while $\hat{\Phi}_{k,\mathrm{N}}$ with density $p_{\mathrm{N}}\lambda_k$ is the transmitter set with NLOS propagation, where $p_{\mathrm{L}} + p_{\mathrm{N}} = 1$ such that $\hat{\Phi}_k = \hat{\Phi}_{k,\mathrm{L}} \cup \hat{\Phi}_{k,\mathrm{N}}$. Then, the interference from tier k can be rewritten as

$$\begin{aligned} I_k &= I_{k,\mathrm{L}} + I_{k,\mathrm{N}} \\ &= \sum_{s\in\{\mathrm{L},\mathrm{N}\}} \sum_{x\in\hat{\Phi}_{k,s}} \mu_k G_k(\varphi_x) h_x \ell_k(x) B_k(x). \end{aligned} \tag{8}$$

Without loss of generality, the noise power is set to one. Conditioning on that the typical receiver belongs to the k-th tier, the corresponding receiver SINR, denoted as SINR_k, is then given by

$$\mathrm{SINR}_k \triangleq \frac{S_k}{1+\sum\limits_{i\in[K]} I_i} = \frac{\mu_k N_k h_{x_0} r_0^{-\alpha_{k,\mathrm{L}}}}{1+\sum\limits_{i\in[K]} \sum\limits_{x\in\hat{\Phi}_i} \mu_i G_i(\varphi_x) h_x \ell_i(x) B_i(x)}, \tag{9}$$

where $[K] \triangleq \{1, 2, ..., K\}$.

The main symbols and parameters are summarized in Table I with default values for the following numerical results.

III. Analysis of the Interference Characteristics

In this section, we derive the mean and variance of the interference for the mm-wave D2D networks and also provide approximations of the interference distribution using a mixture of the inverse gamma and log-normal distributions. The mixture approximation will then be applied in the following section to analyze the SINR and rate distributions.

A. The Mean and Variance of the Interference

Theorem 1. *In the K-tier Poisson mm-wave D2D communication network, the mean interference is*

$$\mathbb{E}(I)=\sum_{i\in[K]}\pi\lambda_i q_i\mu_i \sum_{s\in\{\mathrm{L},\mathrm{N}\}}\frac{p_s(\alpha_{i,s}d_0^{2-\alpha_{i,s}}-2R^{2-\alpha_{i,s}})}{\alpha_{i,s}-2}, \quad (10)$$

and the variance of the interference is

$$\mathbb{V}(I)=\sum_{i\in[K]}\frac{3}{2}\pi\lambda_i q_i\mu_i^2 N_i \sum_{s\in\{\mathrm{L},\mathrm{N}\}} p_s\frac{M_{i,s}+1}{M_{i,s}}\frac{\alpha_{i,s}d_0^{2-2\alpha_{i,s}}-R^{2-2\alpha_{i,s}}}{2(\alpha_{i,s}-1)}. \quad (11)$$

Proof: See Appendix A.

Remark 1. *The expression of the mean interference also applies to general (non-Poisson) heterogeneous networks modeled by multi-tier stationary point processes due to the linearity of the expectation operator. It even holds with inter-tier dependence.*

Theorem 1 leads to some important observations: (1) The mean interference of a multi-tier mm-wave D2D network is independent of the size of the directional antenna array N_i, $i \in [K]$, because the spatial AoD of the interfering signal relative to the typical receiver is randomly distributed and thus the mean interference is constant after averaging over all the directions; (2) Different from the mean, the variance depends on the number of antennas in each tier; (3) Both mean and variance of the interference are proportional to the LOS probability. The intuition behind these observations is that although a larger antenna array forms a narrower beam, which significantly reduces the spread of the interference, once a victim node is affected by this directional transmission beam, the interference suffered is highly detrimental. Thus, after averaging the interference from multiple tiers of transmitters, the mean interference is constant and solely dependent upon the propagation loss while the transmitter density is kept constant. However, the introduction of the heterogeneous antenna arrays has an obvious impact on the variance of the interference, implying large spatial fluctuations of the interference. This phenomenon demonstrates the impact of heterogeneous antenna arrays on the interference distribution and hence the individual link performance.

Fig. 4 illustrates the mean and variance of the aggregate interference for different densities and transmit probabilities, where $K = 3$, $\lambda = 0.3$, $N_1 = 4$, $N_2 = 16$, $N_3 = 64$, and the transmit power is set to 1. It is observed that both mean and variance are proportional to the LOS probability in the mm-wave propagation model. However, compared to the node density and transmit probability, the LOS probability has a much smaller effect on the variance of the interference.

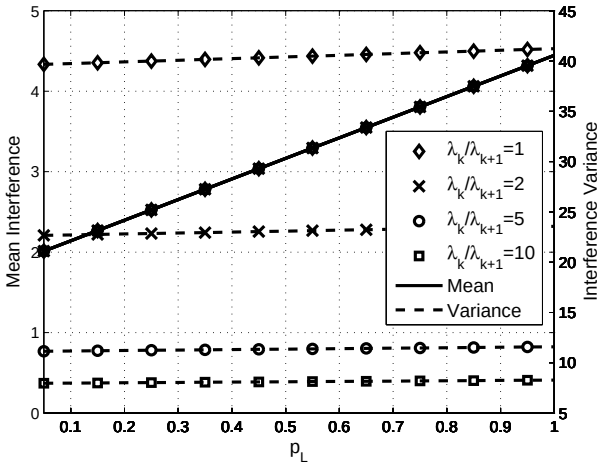

(a) $q_1 = q_2 = q_3 = 1$

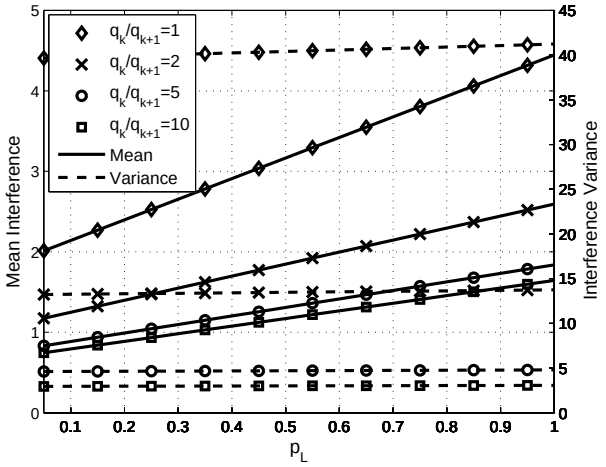

(b) $\lambda_1 = \lambda_2 = \lambda_3 = 0.1$

Fig. 4. The mean and variance of the interference for different densities and transmit probabilities, where $K = 3$, $\lambda = 0.3$, $N_1 = 4$, $N_2 = 16$, $N_3 = 64$ and $\mu_k = 1$, $k \in [K]$.

Moreover, as shown in Fig. 4(a), due to the fixed λ and the same transmit probability in each tier, the active transmitter density $\sum_{i\in[K]}\lambda_i q_i$ is fixed, thus the mean interference stays the same though the densities in different tiers are configured differently. In contrast, Fig. 4(b) considers the case that the transmit probability in each tier is different, leading to the variations of the active transmitter density. In this case, the mean interference for different active transmitter densities is no longer the same, which shows that the transmit probability has an effect on the mean interference, as expected.

B. Approximation of the Interference Distribution

In previous works, three known probability density functions (PDFs), namely the gamma distribution, the inverse Gaussian distribution, and the inverse gamma distribution are examined for modeling the interference distribution [22, 23]. Both the gamma and inverse Gaussian distributions are shown to be suitable for Poisson point process networks while the

inverse gamma distribution is shown to be suitable for Ginibre point process networks, which exhibit repulsion. However, due to the distinguishing channel characteristics of mm-wave communications, such as the distance-dependent path loss with different exponents for LOS and NLOS paths and the sensitivity to blockages leading to severe shadowing effects, the interference characteristics in mm-wave communication networks are rather different from those in conventional networks. For example, in mm-wave networks, we find that it is impossible to use merely one standard PDF to fit the actual interference distribution well since the blockage effect introduces a large variation in the interference power and causes a medium to heavy tail, as shown in Fig. 5. Therefore, in this paper, we introduce a new interference power model—a mixture of the inverse gamma and log-normal distributions—to capture the interference characteristics in mm-wave D2D networks and adopt maximum likelihood estimation (MLE) to estimate the parameters of each of the two standard PDFs. A similar mixture model was presented in [24], but with a mixture of the inverse Gaussian and inverse Weibull distributions.

Specifically, the inverse gamma distribution and log-normal distribution are, respectively, given as follows:

(1) Inverse gamma distribution:

$f_{\mathrm{IG}}(x) = \nu^a x^{-a-1} \exp(-\nu/x)/\Gamma(a)$ with mean $\nu/(a-1)$ and variance $\nu^2/((a-1)^2(a-2))$;

(2) Log-normal distribution:

$f_{\mathrm{LN}}(x) = \frac{1}{x\delta\sqrt{2\pi}} \exp\left(-\frac{(\ln x - \kappa)^2}{2\delta^2}\right)$ with mean $\exp(\kappa + \delta^2/2)$ and variance $(\exp(\delta^2) - 1)\exp(2\kappa + \delta^2)$;

By combining the two distributions, we obtain the mixture model: $f_{\mathrm{MIX}}(x) = \zeta f_{\mathrm{IG}}(x) + (1-\zeta) f_{\mathrm{LN}}(x)$ with $\zeta \in [0, 1]$. Here $f_{\mathrm{MIX}}(x)$ has five unknown parameters, i.e., $\nu, a, \kappa, \delta, \zeta$, which can be obtained by using the `mle` function in Matlab with the sample data from Monte Carlo simulations.

In Fig. 5, we have plotted the PDFs of the interference using Monte Carlo simulation and the three fitted distributions using MLE methods under different network parameter configurations, where $N_1 = 4$, $N_2 = 16$, $N_3 = 64$. For the single-tier case, $N = N_1 = 16$. Although both individual inverse gamma distribution and log-normal distribution give good fits for the interference distribution in sub-6 GHz networks with Rayleigh fading, neither of them is suitable for the approximation of the interference in mm-wave D2D networks with Nakagami fading, whether in the conventional single-tier case or the more general multi-tier case, shown in Fig. 5. The main reason lies in the blockage effect in mm-wave bands, namely the coexistence of different path loss characteristics for LOS and NLOS propagations in mm-wave networks, distinct from conventional networks. In contrast, our proposed mixture distribution outperforms both the individual inverse gamma and log-normal distributions, matching the actual interference distribution extremely well in all three cases. This result aligns with our expectation since the blockage effect causes the interference in the mm-wave networks to be also a combination of the interference from LOS and NLOS transmitters.

We can also see the fitting details of the three distributions from Table II, where two comparisons are given: one is for the mean and the variance between the MLE-based fitted PDFs (see [23, Footnote 4] for a description of the MLE method) and

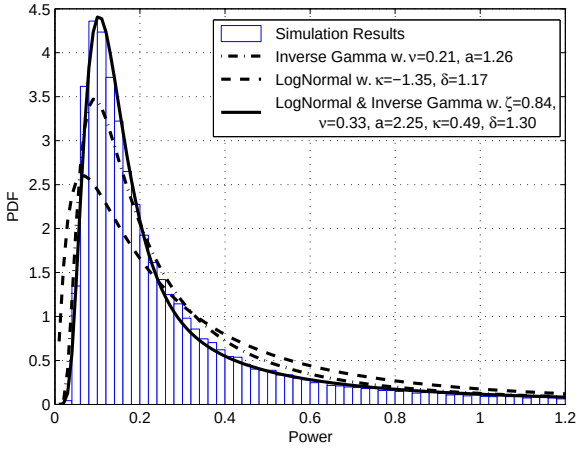

(a) Single-tier network with $\lambda = 0.3$.

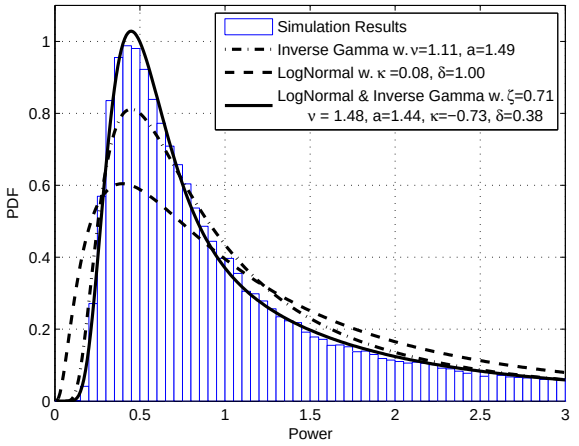

(b) Three-tier network with $\lambda = 0.3$ and $\lambda_i = \lambda_{i+1}$.

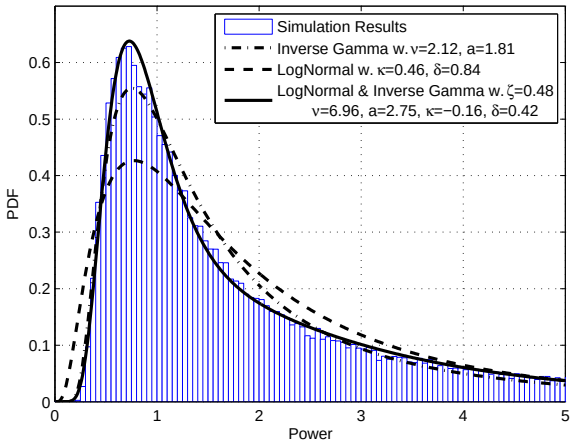

(c) Three-tier network with $\lambda = 0.3$ and $\lambda_i = 5\lambda_{i+1}$.

Fig. 5. Empirical PDF of the interference for the mm-wave D2D networks and the corresponding fits.

TABLE II. Details of interference fitting

Single-tier				
	Empirical	InvGamma	LogNormal	Mix Model
Mean	0.80	0.80	0.52	0.82
Variance	6.7	N/A	0.79	12.1
Log-likelihood	MLE	-8.31×10^3	-2.31×10^4	-5.3×10^3
	TMM	-1.38×10^5	-3.15×10^4	N/A
Three-tier with $\lambda_i=\lambda_{i+1}$				
	Empirical	InvGamma	LogNormal	Mix Model
Mean	2.42	2.29	1.80	2.56
Variance	139.6	N/A	5.7	N/A
Log-likelihood	MLE	-1.41×10^5	-1.51×10^5	-1.40×10^5
	TMM	-1.74×10^5	-1.84×10^5	N/A
Three-tier with $\lambda_i=5\lambda_{i+1}$				
	Empirical	InvGamma	LogNormal	Mix Model
Mean	2.40	2.62	2.26	2.40
Variance	16.7	N/A	5.32	20.0
Log-likelihood	MLE	-1.67×10^5	-1.71×10^5	-1.66×10^5
	TMM	-1.70×10^5	-1.97×10^5	N/A

the simulation results; the other is for the log-likelihood values for the MLE and the so-called two-moment matching (TMM), i.e., setting the mean and the variance of the known distribution to be equal to that of the interference. Since the mixture model has five unknown parameters, the TMM method is unsuitable. Compared with the individual inverse gamma and log-normal distributions, the mixture distribution provides not only the closest approximation (the maximum log-likelihood) to the interference distribution but also the closest variance and similar mean, especially when diverse antenna arrays coexist in a network (i.e., the heterogeneous cases). In addition, since the mixture distribution is a weighted sum of two standard PDFs, it is still very tractable though the complexity is increased slightly.

IV. SINR and Rate Analysis of General mm-Wave D2D Networks

In this section, we first derive the exact results of the SINR and rate distributions in the proposed model for a general mm-wave D2D network with heterogeneous antenna arrays. Then we use two different approaches to simplify the exact results for more efficient calculations: one is to give upper bounds on both the SINR and rate distributions; the other is to provide accurate approximations for the exact results using the fitted interference distribution in Sec. III-B.

A. SINR Distribution

We define the complementary cumulative distribution function (CCDF) of the SINR as

$$P(\theta)=\mathbb{P}(\mathrm{SINR}>\theta), \tag{12}$$

where θ is target SINR threshold. In other works, (12) is referred to as the link success probability [16, 25], which can be thought of equivalently as the probability that the typical user achieves a target SINR θ, or the fraction of users who achieve an SINR of θ in any time slot in any realization of the PPP.

As mentioned in Sec. II-D, we assume that the desired link is in the LOS condition, i.e., $r_0\le R$. Our analytical framework can be easily extended to the general case where the desired signal link is either LOS or NLOS. Given that the desired link is NLOS, the analytical procedure will be the same as the LOS case we consider in this paper. And then, the overall performance can be obtained by using the total probability law, i.e., the SINR CCDF can be expressed as

$$P(\theta)=P_{\mathrm{L}}(\theta)p_{\mathrm{L}}+P_{\mathrm{N}}(\theta)p_{\mathrm{N}}, \tag{13}$$

where P_{L} and P_{N} are the conditional CCDFs on the event that the desired link is LOS and NLOS, respectively.

Our first result in this section is an exact expression for the success probability conditioning on the typical receiver belonging to tier k.

Theorem 2. *Letting $\epsilon_k=\frac{M_{k,\mathrm{L}}r_0^{\alpha_{k,\mathrm{L}}}}{\mu_k N_k}$, the link success probability of the typical active device belonging to the k-th tier equipped with N_k antennas, denoted by $P_k(\theta)$, is given by*

$$P_k(\theta)=\sum_{m=0}^{M_{k,\mathrm{L}}-1}\frac{(-u)^m}{m!}\mathcal{L}^{(m)}(u)|_{u=\theta\epsilon_k}, \tag{14}$$

where $\mathcal{L}(u)=\exp(\eta(u))$, the superscript '$(m)$' stands for the m-th derivative of $\mathcal{L}(u)$, and

$$\eta(u)=-u-\sum_{i\in[K]}\sum_{s\in\{\mathrm{L},\,\mathrm{N}\}}p_s\lambda_i q_i\frac{2}{N_i}\Bigg(\pi R^2 -\int_0^R\int_0^{\frac{\pi}{2}}\frac{M_{i,s}^{M_{i,s}}4r\mathrm{d}x\mathrm{d}r}{\left(M_{i,s}+u\mu_i N_i\cos^2x\max\{r,d_0\}^{-\alpha_{i,s}}\right)^{M_{i,s}}}\Bigg). \tag{15}$$

$\mathcal{L}^{(m)}(u)$ is given recursively by

$$\mathcal{L}^{(m)}(u)=\sum_{n=0}^{m-1}\binom{m-1}{n}\eta^{(m-n)}(u)\mathcal{L}^{(n)}(u), \tag{16}$$

where the n-th derivative of $\eta(u)$ follows

$$\eta^{(n)}(u)=-\mathbf{1}(n=1)+\sum_{i\in[K]}\sum_{s\in\{\mathrm{L},\,\mathrm{N}\}}p_s\lambda_i q_i\frac{8\Gamma(M_{i,s}+n)M_{i,s}^{M_{i,s}}}{N_i\Gamma(M_{i,s})}$$

$$\times\int_0^R\int_0^{\frac{\pi}{2}}\frac{(-\mu_i N_i\cos^2 x\max\{r,d_0\}^{-\alpha_{i,s}})^n r\mathrm{d}x\mathrm{d}r}{\left(M_{i,s}+u\mu_i N_i\cos^2 x\max\{r,d_0\}^{-\alpha_{i,s}}\right)^{M_{i,s}+n}}. \quad (17)$$

Proof: See Appendix B.

From Theorem 2, we obtain a simple relationship between the link success probabilities for different devices when the fading model is the same in all tiers:

Corollary 1. *When $M_{k,\mathrm{L}}=M_{\mathrm{L}}$, $k\in[K]$, letting $A_k=\mu_k N_k/r_0^{\alpha_{k,\mathrm{L}}}$ and*

$$P_{\mathrm{base}}(\theta)=\sum_{m=0}^{M_{\mathrm{L}}-1}\frac{(-u)^m}{m!}\mathcal{L}^{(m)}(u)|_{u=\theta M_{\mathrm{L}}}, \quad (18)$$

we have $P_k(\theta)=P_{\mathrm{base}}(\theta/A_k)$, which means the link success probabilities for different kinds of devices can be characterized by a horizontal shift (in dB) of the baseline curve (18).

The following corollary gives the asymptotic behavior of the SINR distribution of the typical active receiver, which provides a simple yet effective way to quantify how close the SINR distributions are.

Corollary 2. *For the typical active device equipped with N_k antennas, the asymptotic behavior for the link success probability is*

$$P_k(\theta)\sim 1-\theta^{M_{k,\mathrm{L}}}\frac{(-\epsilon_k)^{M_{k,\mathrm{L}}}}{\Gamma(M_{k,\mathrm{L}}+1)}\mathcal{L}^{(M_{k,\mathrm{L}})}(0),\quad \theta\to 0. \quad (19)$$

Proof: For the typical active device equipped with N_k antennas, the link success probability $P_k(\theta)$ is expressed as

$$\begin{aligned}P_k(\theta)&=\mathbb{P}\left(\frac{\mu_k N_k h_{x_0} r_0^{-\alpha_{k,\mathrm{L}}}}{1+I}>\theta\right)\\&=1-\mathbb{E}\left[\widetilde{\gamma}\left(M_{k,\mathrm{L}},\theta\epsilon_k(1+I)\right)\right]\\&\sim 1-\frac{1}{\Gamma(M_{k,\mathrm{L}})M_{k,\mathrm{L}}}\mathbb{E}\left[\left(\theta\epsilon_k(1+I)\right)^{M_{k,\mathrm{L}}}\right],\ \theta\to 0\\&\sim 1-\theta^{M_{k,\mathrm{L}}}\frac{\epsilon_k^{M_{k,\mathrm{L}}}}{\Gamma(M_{k,\mathrm{L}}+1)}\mathbb{E}\left[(1+I)^{M_{k,\mathrm{L}}}\right],\ \theta\to 0, \quad (20)\end{aligned}$$

where $\widetilde{\gamma}(x,y)=\gamma(x,y)/\Gamma(x)$ is the normalized lower incomplete gamma function, and

$$\mathbb{E}\left[(1+I)^{M_{k,\mathrm{L}}}\right]=(-1)^{M_{k,\mathrm{L}}}\mathcal{L}^{(M_{k,\mathrm{L}})}(u)|_{u=0}. \quad (21)$$

■

From (19), we know that the asymptote of the outage probability for the k-th tier device is expressed as

$$1-P_k(\theta)\sim\xi\theta^{M_{k,\mathrm{L}}},\quad \theta\to 0, \quad (22)$$

where $M_{k,\mathrm{L}}$ is the asymptotic slope and the pre-constant $\xi=\frac{(-\epsilon_k)^{M_{k,\mathrm{L}}}}{\Gamma(M_{k,\mathrm{L}}+1)}\mathcal{L}^{(M_{k,\mathrm{L}})}(0)$ characterizes the horizontal gap between the SINR distributions for the devices in different tiers if they have the same asymptotic slope $M_{k,\mathrm{L}}$. Such horizontal gaps quantify the effect of the parameters, such as the transmit power, path loss exponent, antenna array size, etc., on the SINR performance.

Note that both the two above corollaries characterize gaps between SINR distributions: Corollary 1 is a shifting result for all values of θ for the case when the Nakagami parameter is the same in all tiers; while Corollary 2 gives an asymptotic shifting result for arbitrary Nakagami parameters as $\theta\to 0$.

According to the proposed model, devices in different tiers differ in the number of antennas and follow multiple mutually independent homogeneous PPPs. Therefore, the total SINR distribution of the mm-wave D2D network can be computed using the law of total probability as follows.

Corollary 3. *For the overall active user, the link success probability is*

$$P(\theta)=\sum_{k\in[K]}\frac{\lambda_k q_k}{\sum_{i\in[K]}\lambda_i q_i}P_k(\theta). \quad (23)$$

Proof: Let us consider the point process of all active receivers (those who have active transmitters) and focus on the typical receiver of this point process. Based on Theorem 2, which gives the link success probability conditioned on this typical receiver belonging to the k-th tier, the overall link success probability is obtained as

$$P(\theta)=\sum_{k\in[K]}\mathbb{P}(x\in\hat{\Phi}_k)P_k(\theta), \quad (24)$$

where $\mathbb{P}(x\in\hat{\Phi}_k)$ is the probability that the typical receiver belongs to the k-th tier. Since $\mathbb{P}(x\in\hat{\Phi}_k)=\frac{\lambda_k q_k}{\sum_{i\in[K]}\lambda_i q_i}$, we obtain (23). ■

Note that though the Laplace transform of the aggregate interference can be easily evaluated by numerical integration, the corresponding n-th derivative needs tedious and extensive computations, which makes the exact calculation inefficient. Thus, in the following two subsections, we will simplify the exact results by means of bounding and approximating, respectively.

1) Bounds on SINR Distribution: Using bounds of the incomplete gamma functions, we obtain upper and lower bounds for the link success probability as follows.

Theorem 3. *Let $\beta_k=[\Gamma(1+M_{k,\mathrm{L}})]^{-1/M_{k,\mathrm{L}}}$ and*

$$\hat{P}_k(\theta)=\sum_{m=1}^{M_{k,\mathrm{L}}}\binom{M_{k,\mathrm{L}}}{m}(-1)^{m+1}\mathcal{L}(u)\big|_{u=m\theta\beta_k\epsilon_k}. \quad (25)$$

For K-tier Poisson mm-wave D2D communication networks, the link success probability of the active device belonging to the k-th tier $P_k(\theta)$ is upper bounded by $\hat{P}_k(\theta)$, while a lower bound on $P_k(\theta)$, denoted by $\check{P}_k(\theta)$, is achieved by setting $\beta_k=1$ in (25), i.e.,

$$\check{P}_k(\theta)=\sum_{m=1}^{M_{k,\mathrm{L}}}\binom{M_{k,\mathrm{L}}}{m}(-1)^{m+1}\mathcal{L}(u)\big|_{u=m\theta\epsilon_k}. \quad (26)$$

Proof: It is known from [26] that

$$1-[1-\exp(-x)]^M\le\widetilde{\Gamma}(M,x)\le 1-[1-\exp(-\beta x)]^M, \quad (27)$$

where $\beta=[\Gamma(1+M)]^{-1/M}$, $\widetilde{\Gamma}(M,x)=\Gamma(M,x)/\Gamma(M)$, and the equality holds only if $M=1$. Based on this inequality, the lower and upper bounds on the link success probability

are obtained as follows. Letting $\beta_k = [\Gamma(1+M_{k,\mathrm{L}})]^{-1/M_{k,\mathrm{L}}}$ and $\hat{P}_k(\theta)$ be the upper bound on $P_k(\theta)$, we have

$$\begin{aligned}\hat{P}_k(\theta) =& 1-\mathbb{E}\left[\left(1-\exp\left(-\theta\beta_k\epsilon_k(1+I)\right)\right)^{M_{k,\mathrm{L}}}\right]\\ =&\sum_{m=1}^{M_{k,\mathrm{L}}}\binom{M_{k,\mathrm{L}}}{m}(-1)^{m+1}\mathbb{E}\left[\exp\left(-m\theta\beta_k\epsilon_k(1+I)\right)\right]\\ =&\sum_{m=1}^{M_{k,\mathrm{L}}}\binom{M_{k,\mathrm{L}}}{m}(-1)^{m+1}\mathcal{L}(u)\big|_{u=m\theta\beta_k\epsilon_k}. \end{aligned} \tag{28}$$

By substituting (15) into (28), we obtain the upper bound for the link success probability. From (27), the lower bound for the link success probability $\check{P}_k(\theta)$ is then obtained by setting $\beta_k = 1$ in (28). ∎

Remark 2. *Compared with the exact results for the SINR distribution, both bounds give much simpler expressions without requiring the derivatives for $\mathcal{L}(u)$ at $u \neq 0$, where $\mathcal{L}(u)$ is the product of multiple exponential functions with integral expressions in the exponents. Thus the effort for the computation of the SINR distribution is significantly reduced.*

In order to provide a simple and rigorous quantitative result on the tightness of the bounds, we also analyze the asymptotic behavior of the lower and upper bounds as $\theta \to 0$ in the following corollary.

Corollary 4. *For the typical active device equipped with N_k antennas, the asymptotic behavior for the bounds of the link success probability is*

$$\hat{P}_k(\theta) \sim 1-\theta^{M_{k,\mathrm{L}}}\frac{(-\epsilon_k)^{M_{k,\mathrm{L}}}}{\Gamma(M_{k,\mathrm{L}}+1)}\mathcal{L}^{(M_{k,\mathrm{L}})}(0), \quad \theta\to 0, \tag{29}$$

$$\check{P}_k(\theta) \sim 1-\theta^{M_{k,\mathrm{L}}}(-\epsilon_k)^{M_{k,\mathrm{L}}}\mathcal{L}^{(M_{k,\mathrm{L}})}(0), \quad \theta\to 0. \tag{30}$$

Proof: For the typical active device equipped with N_k antennas, the upper bound for the link success probability $\hat{P}_k(\theta)$ is expressed as

$$\begin{aligned}\hat{P}_k(\theta) =& 1-\mathbb{E}\left[\left(1-\exp\left(-\theta\beta_k\epsilon_k(1+I)\right)\right)^{M_{k,\mathrm{L}}}\right]\\ \sim& 1-\mathbb{E}\left[\left(\theta\beta_k\epsilon_k(1+I)\right)^{M_{k,\mathrm{L}}}\right], \quad \theta\to 0\\ \sim& 1-\theta^{M_{k,\mathrm{L}}}(\beta_k\epsilon_k)^{M_{k,\mathrm{L}}}\mathbb{E}(1+I)^{M_{k,\mathrm{L}}}, \quad \theta\to 0\\ \sim& 1-\theta^{M_{k,\mathrm{L}}}\frac{(-\epsilon_k)^{M_{k,\mathrm{L}}}}{\Gamma(M_{k,\mathrm{L}}+1)}\mathcal{L}^{(M_{k,\mathrm{L}})}(0), \quad \theta\to 0. \end{aligned} \tag{31}$$

The asymptotic behavior of the lower bound $\check{P}_k(\theta)$ is obtained analogously by setting $\beta_k = 1$. ∎

Remark 3. *The asymptotic behavior of the upper bound is the same as that of the exact result, which validates the efficiency and accuracy of the upper bound. Moreover, as $\theta \to 0$, the asymptotic slope of $\log(1-P_k(\theta))$ is the Nakagami fading parameter $M_{k,\mathrm{L}}$, and we have $P_k(\theta) \sim \hat{P}_k(\theta) \sim \check{P}_k(\theta/\vartheta)$ where $\vartheta = \Gamma(M_{k,\mathrm{L}}+1)^{1/M_{k,\mathrm{L}}}$. These are validated in Fig. 6, where the asymptotic slope is 4 since $M_{k,\mathrm{L}} = 4$.*

Similar to the exact results, we can obtain bounds for the overall link success probability by Corollary 3.

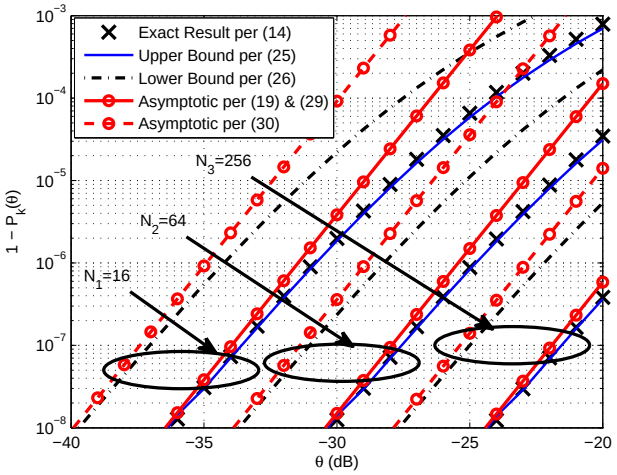

Fig. 6. The asymptotic SINR CDF for each tier with $K = 3$, $M_{k,\mathrm{L}} = 4$, $k \in [K]$, $N_1 = 16$, $N_2 = 64$, and $N_3 = 256$.

2) Approximation by Interference Distribution: Based on the fitted interference distribution in Sec. III-B, we obtain an approximation of the link success probability for the k-th tier, given by

$$\widetilde{P}_k(\theta) \triangleq \int_0^\infty \widetilde{\Gamma}\Big(M_{k,\mathrm{L}}, \theta\epsilon_k(1+x)\Big) f_{\mathrm{MIX}}(x)\mathrm{d}x. \tag{32}$$

$\widetilde{P}_k(\theta)$ is the approximative success probability since

$$\begin{aligned} P_k(\theta) =& \mathbb{E}\left[\widetilde{\Gamma}\Big(M_{k,\mathrm{L}}, \theta\epsilon_k(1+I)\Big)\right]\\ =& \int_0^\infty \widetilde{\Gamma}\Big(M_{k,\mathrm{L}}, \theta\epsilon_k(1+x)\Big) f_I(x)\mathrm{d}x\\ \approx& \int_0^\infty \widetilde{\Gamma}\Big(M_{k,\mathrm{L}}, \theta\epsilon_k(1+x)\Big) f_{\mathrm{MIX}}(x)\mathrm{d}x\\ =& \widetilde{P}_k(\theta). \end{aligned} \tag{33}$$

Note that $\widetilde{P}_k(\theta)$ can be easily evaluated by numerical integration and thus significantly improves the evaluation efficiency without calculating the derivatives once $f_{\mathrm{MIX}}(x)$ is known. Similar to the exact results, we can obtain the approximation for the overall link success probability by Corollary 3.

Fig. 7 illustrates the link success probability as a function of θ for different configurations of antenna arrays in a 3-tier mm-wave D2D network. It can be seen that the upper bound (25) derived for the success probability is tight and the approximation using the fitted mixture model of interference distribution matches extremely well. The lower bound (26), though it is not very tight, the horizontal gap between the bounds and the exact curve is nearly constant, with the upper bound less than 0.5 dB and the lower bound about 2.2 dB away. Moreover, it is also observed that the configuration with larger antenna arrays performs better in terms of the link success probability, since larger antenna arrays produce narrower transmission beams, which limit the interference signal to a certain direction, causing less interference to the receivers. Comparing the curves corresponding to the combinations of antenna arrays $[4, 64, 256]$ and $[16, 64, 256]$, there is a critical

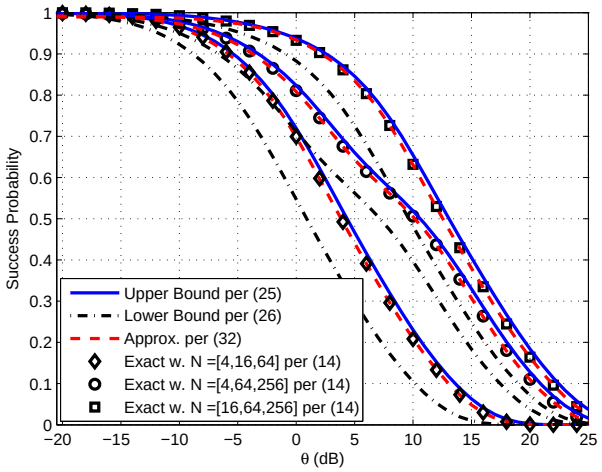

Fig. 7. The success probability for different configurations of antenna arrays with $K = 3$.

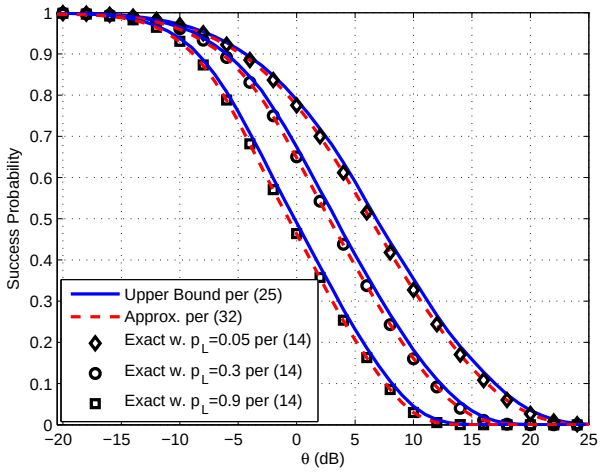

Fig. 8. The success probability for different LOS probabilities with $K = 3$.

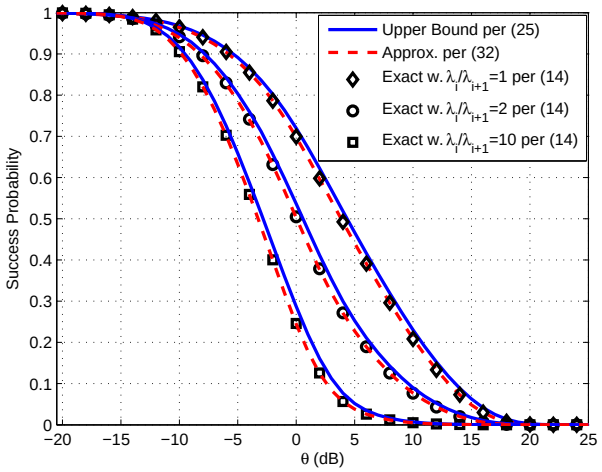

Fig. 9. The success probability for different density ratios for $K = 3$.

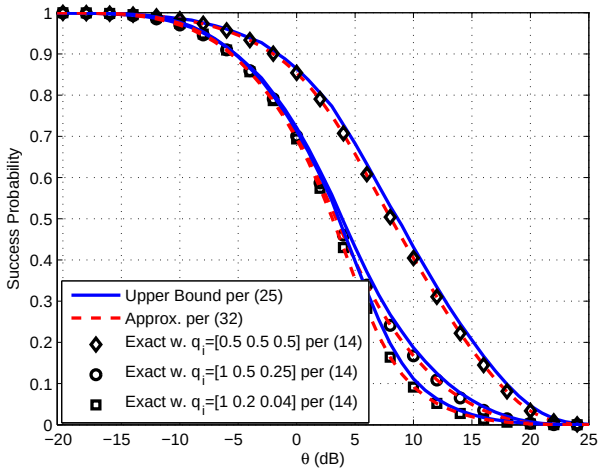

Fig. 10. Effect of transmit probability on link success probability for $K = 3$.

point at $\theta = 10$ dB, where the link success probability with $[4, 64, 256]$ is quite close to but smaller than that with $[16, 64, 256]$. This is because when the SINR threshold is large, the successful transmissions mostly occur at the transmitters with larger antenna arrays (e.g., $N_3 = 256$). In this case, the desired signal between two cases is almost at the same level while the interference suffered in the case of $N = [4\ 64\ 256]$ is more severe than that in the case of $N = [16\ 64\ 256]$.

Fig. 8 shows the impact of the LOS probability p_{L} on the link success probability in a 3-tier mm-wave D2D network, where $N_1 = 4$, $N_2 = 16$, and $N_3 = 64$. It is observed that the link success probability deteriorates with the increase of p_{L}. The reason is that a high LOS probability means the propagation environment suffers from less blockage and, accordingly, the interfering signals experience less propagation loss than in the blocked case. As a result, the aggregate interference at receivers will become more severe, thereby decreasing the link success probability.

Fig. 9 shows the relationship between the density ratios in different tiers and the link success probability in a 3-tier mm-wave D2D network where $\lambda = 0.3$, $N_1 = 4$, $N_2 = 16$ and $N_3 = 64$. We can see that the best performance in the three cases is achieved when the tier with the largest antenna array $N_3 = 64$ is configured with the biggest density, i.e., $\lambda_3 = 0.1$. The reason is that larger antenna arrays can form narrower beams, which usually give better desired signal strength and cause less interference, and thus the overall performance improves when more devices are configured with larger antenna arrays.

Fig. 10 investigates the impact of the transmit probabilities on the link success probability in a 3-tier mm-wave D2D network where $\lambda = 0.3$, $N_1 = 4$, $N_2 = 16$ and $N_3 = 64$. It is seen that devices with a larger antenna array and transmit probability can achieve better performance. Actually, since the link success probability represents an average over all the links in a single realization if the point process is ergodic, it is determined by the active transmitter density $\lambda_i q_i$ in each tier, where $i \in [K]$. Thus, keeping the density constant and changing the transmit probability in each tier is equivalent to keeping the transmit probability constant while changing the

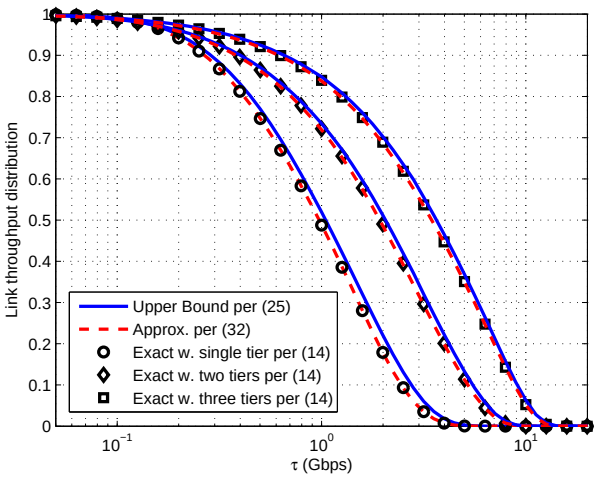

Fig. 11. Rate distribution for different numbers of tiers K.

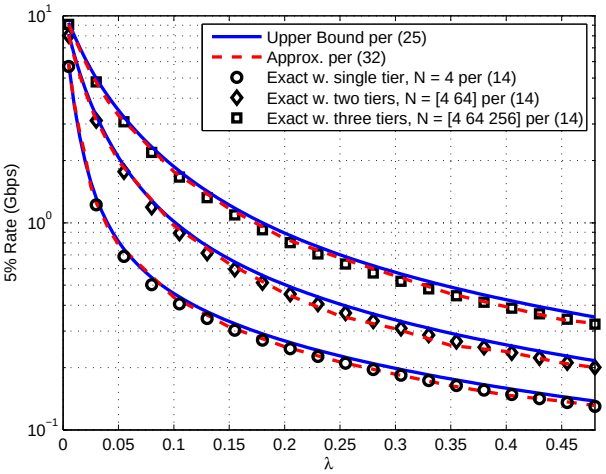

Fig. 12. 5% rates as a function of the overall density λ.

density in terms of the success probability given fixed overall transmitter density.

B. Rate Distribution

In addition to the transmission reliability (i.e., the success probability), the data rate, characterized by the rate distribution $\mathcal{T}(\tau) = \mathbb{P}(T > \tau)$, is another important performance metric since it directly affects the perceived user experience. T represents the (random) data rate per active user, in units of either bits per second (bps) or bps/Hz if the bandwidth W is normalized. According to the Shannon capacity formula $T = W \log_2(1 + \mathrm{SINR})$ and the SINR distribution derived in the previous subsection, the rate distribution of the typical active user belonging to the k-th tier can be computed straightforwardly through $\mathbb{P}(W \log_2(1+\mathrm{SINR}_k) > \tau) = P_k(2^{\tau/W} - 1)$. Similar to the calculation of the overall SINR distribution in (23), we obtain the rate distribution of the typical user as

$$\mathcal{T}(\tau) = \sum_{k\in[K]} \frac{\lambda_k q_k}{\sum_{i\in[K]} \lambda_i q_i} P_k(2^{\tau/W} - 1). \tag{34}$$

Then, bounds and an approximation of the rate distribution can be obtained by replacing $P_k(2^{\tau/W} - 1)$ by $\hat{P}_k(2^{\tau/W} - 1)$ and $\tilde{P}_k(2^{\tau/W} - 1)$, respectively.

The rate distribution is shown in Fig. 11 for different numbers of tiers, which, equivalently, can be explained as different degrees of diversification in antenna arrays. For each curve, the total density $\lambda = 0.3$, and the densities of different tiers are equal if $K > 1$. The simulation and the fitted approximation are based on the actual antenna pattern while the bound is based on the cosine antenna pattern. It is observed that the upper bound is tight for the simulation result and the approximation using the fitted mixture model of interference distribution matches well, which further verifies the effectiveness of the cosine antenna pattern approximation in terms of the rate distribution. In addition, with the gradual introduction of devices equipped with large antenna arrays, e.g., from the single-tier network composed of solely 4-antenna devices to the three-tier network where devices equipped with 4, 16, 64 antennas coexist, the rate gain is significantly improved. Specifically, we find that at least 70% and 85% of the users achieve a rate of 1 Gbps after introducing the 16-antenna and 64-antenna devices, respectively, which demonstrates the advantages of the multi-antenna techniques for mm-wave D2D communications.

Fig. 12 evaluates the performance of the devices achieving the worst 5% rate with the increase of density λ, where we define the 5% rate as the rate τ with $\mathcal{T}(\tau) = 0.95$. It is shown that both the upper bound and the approximation match the simulation result well. Moreover, the 5% rate decreases sharply as the density start to increase and gently when $\lambda > 0.1$. Since we focus on the point-to-point rate, increasing the density means increasing the concurrent transmitters and hence the aggregate interference in the network. For different combinations of antenna arrays, the maximum density that maintains the 5% rate at more than 1 Gbps is different, where this 1 Gbps can be referred as a QoS requirement. For $N = [4, 64, 256]$, the maximum density under this requirement is about $0.16\,\mathrm{m}^{-2}$ while for $N = 4$, it is less than $0.05\,\mathrm{m}^{-2}$. These observations indicate the importance of adopting large antenna arrays in mm-wave communications to drastically reduce the interference to those receivers most strongly affected by the interference, but the overall density should be controlled in a certain range (i.e., less than the maximum density given a rate requirement).

V. Conclusions

In this paper, we proposed a general and tractable framework for the performance analysis in mm-wave D2D network where devices are diversified in their directional antenna arrays. We first investigated the interactions between beams formed by the transmitters with different numbers of antennas. Interestingly, we found that the first side lobe gain of a larger antenna array can be close to the main lobe gain of a smaller one merely in a limited spatial direction. Considering both accuracy and tractability, the cosine antenna pattern was adopted as the antenna model. It turns out that the mean interference is independent of the size of directional antenna array while the variance is not; and both the mean and variance

are proportional to the LOS probability. Using the maximum likelihood estimation, we also provided approximations of the interference distribution using the inverse gamma distribution, the log-normal distribution and their combinations. Through comparison with Monte Carlo simulations, we observed that our proposed mixture model outperforms the individual inverse gamma and log-normal distributions, matching the actual interference extremely well.

Furthermore, using this framework, we derived the SINR and rate distributions of the typical receiver. To improve the evaluation efficiency, we also provided tight bounds and approximations with good accuracy to simplify the exact results. It was observed that the introduction of large antenna arrays in mm-wave networks bring immense benefits in terms of both reliability (success probability) and effectiveness (rate), especially for the worst 5% users, which can not only improve the desired signal but also significantly reduce the interference.

In summary, different from the existing works where all the network nodes are equipped with the same antenna arrays, more realistically, we focus on the heterogeneity of devices in a mm-wave D2D network and analyze the impact of directional antenna arrays on the performance, which provides valuable engineering insights to help network operators deploy D2D communication in mm-wave bands.

Appendix A
Proof of Theorem 1

Proof: The aggregate interference of the typical receiver is given by $I = \sum_{i\in[K]} I_i$ and we have $\mathbb{E}(I) = \sum_{i\in[K]} \mathbb{E}(I_i)$. The mean interference from tier i is expressed as

$$\begin{aligned}\mathbb{E}(I_i) &= \mathbb{E}_{\hat{\Phi}_i}\Big(\mathbb{E}\sum_{x\in\hat{\Phi}_i}\mu_i G_i(\varphi_x)h_x\ell_i(x)B_i(x)\mid\hat{\Phi}_i\Big)\\ &= q_i\mu_i\mathbb{E}_{\hat{\Phi}_i}\Big(\sum_{x\in\hat{\Phi}_i}\ell_i(x)\Big)\int_{-\frac{1}{N_i}}^{\frac{1}{N_i}} N_i\cos^2\Big(\frac{\pi N_i}{2}\varphi\Big)\mathrm{d}\varphi\\ &\overset{(a)}{=} q_i\mu_i\lambda_i\Big(p_{\mathrm{L}}\int_{b(o,R)}(\max\{|x|,d_0\})^{-\alpha_{i,\mathrm{L}}}\mathrm{d}x\\ &\quad+p_{\mathrm{N}}\int_{b(o,R)}(\max\{|x|,d_0\})^{-\alpha_{i,\mathrm{N}}}\mathrm{d}x\Big)\\ &= \pi\lambda_i q_i\mu_i\sum_{s\in\{\mathrm{L},\mathrm{N}\}}\frac{p_s(\alpha_{i,s}d_0^{2-\alpha_{i,s}}-2R^{2-\alpha_{i,s}})}{\alpha_{i,s}-2},\end{aligned}\tag{35}$$

where $b(o,R)$ denotes the disk centered at the origin with radius R and step (a) uses Campbell's theorem [19, Thm. 4.1]. Therefore, the mean aggregate interference suffered by the typical receiver is obtained by substituting (35) into $\mathbb{E}(I) = \sum_{i\in[K]}\mathbb{E}(I_i)$.

Due to the independence of the PPPs $\hat{\Phi}_i$, $i\in[K]$, and the blockage model, the variance of the aggregate interference is

$$\mathbb{V}(I) = \sum_{i\in[K]}\mathbb{V}(I_i) = \sum_{i\in[K]}\sum_{s\in\{\mathrm{L},\mathrm{N}\}}\mathbb{V}(I_{i,s}).\tag{36}$$

We first calculate the variance of the interference from the LOS transmitters in the i-th tier, i.e., $\mathbb{V}(I_{i,\mathrm{L}})$, expressed as

$$\mathbb{V}(I_{i,\mathrm{L}}) = \mathbb{E}[(I_{i,\mathrm{L}})^2] - (\mathbb{E}I_{i,\mathrm{L}})^2.\tag{37}$$

The first term of (37) is given by

$$\begin{aligned}\mathbb{E}[(I_{i,\mathrm{L}})^2] &= \mathbb{E}\Big(\sum_{x\in\hat{\Phi}_{i,\mathrm{L}}}\mu_k G_k(\varphi_x)h_x\ell_k(x)B_k(x)\Big)^2\\ &= \mathbb{E}\Big(\sum_{x\in\hat{\Phi}_{i,\mathrm{L}}}\Big(\mu_k G_i(\varphi_x)h_x\ell_i(x)B_i(x)\Big)^2\\ &\quad+\sum_{\substack{x,y\in\hat{\Phi}_{i,\mathrm{L}}\\ x\neq y}}\mu_k^2 G_k(\varphi_x)G_k(\varphi_y)h_xh_y\ell_i(x)\ell_i(y)B_i(x)B_i(y)\Big)\\ &\overset{(b)}{=} q_i\mu_i^2\frac{M_{i,\mathrm{L}}+1}{M_{i,\mathrm{L}}}\mathbb{E}_{\hat{\Phi}_{i,\mathrm{L}}}\sum_{x\in\hat{\Phi}_{i,\mathrm{L}}}\ell_i^2(x)\int_{-\frac{1}{N_i}}^{\frac{1}{N_i}}N_i^2\cos^4\Big(\frac{\pi N_i}{2}\varphi\Big)\mathrm{d}\varphi\\ &\quad+p_i^2\mu_i^2\mathbb{E}_{\hat{\Phi}_{i,\mathrm{L}}}\sum_{\substack{x,y\in\hat{\Phi}_{i,\mathrm{L}}\\ x\neq y}}\ell_i(x)\ell_i(y)\\ &\overset{(c)}{=} q_i\mu_i^2\frac{M_{i,\mathrm{L}}+1}{M_{i,\mathrm{L}}}\frac{3}{4}N_i 2\pi p_{\mathrm{L}}\lambda_i\int_0^R(\max\{r,d_0\})^{-2\alpha_{i,\mathrm{L}}}r\mathrm{d}r\\ &\quad+p_i^2\mu_i^2(2\pi p_{\mathrm{L}}\lambda_i)^2\int_0^R\int_0^R(\max\{r_1,d_0\})^{-\alpha_{i,\mathrm{L}}}\\ &\quad\times(\max\{r_2,d_0\})^{-\alpha_{i,\mathrm{L}}}r_1r_2\mathrm{d}r_1\mathrm{d}r_2\\ &= \frac{3}{2}q_i\mu_i^2\frac{M_{i,\mathrm{L}}+1}{M_{i,\mathrm{L}}}N_i\pi p_{\mathrm{L}}\lambda_i\int_0^R(\max\{r,d_0\})^{-2\alpha_{i,\mathrm{L}}}r\mathrm{d}r\\ &\quad+(\mathbb{E}I_{i,\mathrm{L}})^2,\end{aligned}\tag{38}$$

where step (b) uses $\mathbb{E}h_x^2 = \frac{1+M_{i,\mathrm{L}}}{M_{i,\mathrm{L}}}$ since h_x follows the gamma distribution $\mathrm{Gamma}(M_{i,\mathrm{L}}, \frac{1}{M_{i,\mathrm{L}}})$, and step (c) follows from Campbell's theorem and the second-order product density [19, Def. 6.4] of the PPP. As a result, we have

$$\mathbb{V}(I_{i,\mathrm{L}}) = \frac{3}{2}\pi N_i q_i\lambda_i\mu_i^2\frac{M_{i,\mathrm{L}}+1}{M_{i,\mathrm{L}}}p_{\mathrm{L}}\frac{\alpha_{i,\mathrm{L}}d_0^{2-2\alpha_{i,\mathrm{L}}}-R^{2-2\alpha_{i,\mathrm{L}}}}{2(\alpha_{i,\mathrm{L}}-1)}.\tag{39}$$

Similarly, we derive the variance of the interference from the NLOS transmitters in the i-th tier as

$$\mathbb{V}(I_{i,\mathrm{N}}) = \frac{3}{2}\pi N_i q_i\lambda_i\mu_i^2\frac{M_{i,\mathrm{N}}+1}{M_{i,\mathrm{N}}}p_{\mathrm{N}}\frac{\alpha_{i,\mathrm{N}}d_0^{2-2\alpha_{i,\mathrm{N}}}-R^{2-2\alpha_{i,\mathrm{N}}}}{2(\alpha_{i,\mathrm{N}}-1)}.\tag{40}$$

and the variance of the aggregate interference is obtained by substituting (39) and (40) into (36). ■

Appendix B
Proof of Theorem 2

Proof: The link success probability of a device belonging to the k-th tier, denoted by $P_k(\theta)$, is expressed as

$$P_k(\theta) = \mathbb{P}\left(\frac{\mu_k N_k h_{x_0} r_0^{-\alpha_{k,\mathrm{L}}}}{1+I} > \theta\right)$$

$$= \mathbb{E}\left[\widetilde{\Gamma}\left(M_{k,\mathrm{L}}, \theta\epsilon_k(1+I)\right)\right]$$
$$= \sum_{m=0}^{M_{k,\mathrm{L}}-1} \mathbb{E}\left[e^{-\theta\epsilon_k(1+I)}\frac{(\theta\epsilon_k(1+I))^m}{m!}\right]$$
$$= \sum_{m=0}^{M_{k,\mathrm{L}}-1} \frac{(-u)^m}{m!}\mathcal{L}^{(m)}(u)|_{u=\theta\epsilon_k}$$

where $\widetilde{\Gamma}(x,y) = \Gamma(x,y)/\Gamma(x)$ is the normalized incomplete gamma function, $\mathcal{L}(u) = \mathbb{E}[e^{-u(I+1)}]$ is the Laplace transform of the interference and noise, and the superscript (m) stands for the m-th derivative of $\mathcal{L}(u)$. Due to the independence of the K tiers, we have

$$\mathcal{L}(u) = e^{-u}\prod_{i\in[K]}\prod_{s\in\{\mathrm{L},\,\mathrm{N}\}}\mathcal{L}_{I_{i,s}}(u), \tag{41}$$

where $\mathcal{L}_{I_{i,s}}(u)$ follows as

$$\begin{aligned}\mathcal{L}_{I_{i,s}}(u) =& \mathbb{E}\left[\exp\left(-u\sum_{x\in\hat{\Phi}_{i,s}}\mu_i G_i(\varphi_x)h_x\ell_i(x)B_i(x)\right)\right]\\ =& \mathbb{E}\left[\prod_{x\in\hat{\Phi}_{i,s}}\left(\frac{q_i}{\left(1+\frac{u\mu_i}{M_{i,s}}G_i(\varphi_x)\ell_i(x)\right)^{M_{i,s}}}+1-q_i\right)\right]\\ =& \mathbb{E}_{\hat{\Phi}_{i,s}}\left[\prod_{x\in\hat{\Phi}_{i,s}}\left(\int_{\frac{1}{N_i}}^{\frac{1}{N_i}}\frac{q_i\mathrm{d}\varphi}{\left(1+\frac{u\mu_i N_i}{M_{i,s}}\cos^2\left(\frac{\pi N_i}{2}\varphi\right)\ell_i(x)\right)^{M_{i,s}}}\right.\right.\\ &\left.\left.+1-\frac{2q_i}{N_i}\right)\right]\\ =& \exp\left(-p_s\lambda_i q_i\frac{2}{N_i}\left(\pi R^2\right.\right.\\ &\left.\left.-\int_0^R\int_0^{\frac{\pi}{2}}\frac{4r\mathrm{d}x\mathrm{d}r}{\left(1+\frac{u\mu_i N_i}{M_{i,s}}\cos^2 x\max\{r,d_0\}^{-\alpha_{i,s}}\right)^{M_{i,s}}}\right)\right)\end{aligned} \tag{42}$$

Letting

$$\begin{aligned}\eta(u) =& -u-\sum_{i\in[K]}\sum_{s\in\{\mathrm{L},\,\mathrm{N}\}}p_s\lambda_i q_i\frac{2}{N_i}\left(\pi R^2\right.\\ &\left.-\int_0^R\int_0^{\frac{\pi}{2}}\frac{M_{i,s}^{M_{i,s}}4r\mathrm{d}x\mathrm{d}r}{\left(M_{i,s}+u\mu_i N_i\cos^2 x\max\{r,d_0\}^{-\alpha_{i,s}}\right)^{M_{i,s}}}\right),\end{aligned} \tag{43}$$

we have $\mathcal{L}(u) = \exp(\eta(u))$. Since $\mathcal{L}^{(1)}(u) = \eta^{(1)}(u)\mathcal{L}(u)$, $\mathcal{L}^{(m)}(u)$ can be calculated recursively according to the formula of Leibniz for the higher-order derivative of the product of two functions, given by

$$\mathcal{L}^{(m)}(u) = \frac{\mathrm{d}^{m-1}}{\mathrm{d}u}\mathcal{L}^{(1)}(u) = \sum_{n=0}^{m-1}\binom{m-1}{n}\eta^{(m-n)}(u)\mathcal{L}^{(n)}(u), \tag{44}$$

where the n-th derivative of $\eta(u)$ follows as

$$\eta^{(n)}(u) = -\mathbf{1}(n=1) + \sum_{i\in[K]}\sum_{s\in\{\mathrm{L},\,\mathrm{N}\}}p_s\lambda_i q_i\frac{8\Gamma(M_{i,s}+n)M_{i,s}^{M_{i,s}}}{N_i\Gamma(M_{i,s})}$$
$$\times\int_0^R\int_0^{\frac{\pi}{2}}\frac{(-\mu_i N_i\cos^2 x\max\{r,d_0\}^{-\alpha_{i,s}})^n r\mathrm{d}x\mathrm{d}r}{\left(M_{i,s}+u\mu_i N_i\cos^2 x\max\{r,d_0\}^{-\alpha_{i,s}}\right)^{M_{i,s}+n}}. \tag{45}$$

■

REFERENCES

[1] N. Deng, Y. Sun, and M. Haenggi, "Success probability of millimeter-wave D2D networks with heterogeneous antenna arrays," in *IEEE Wireless Communications and Networking Conference (WCNC'18)*, Barcelona, Spain, Apr. 2018.

[2] Cisco, "Cisco visual networking index: Global mobile data traffic forecast update, 2016-2021," http://www.cisco.com/c/en/us/solutions/collateral/service-provider/visual-networking-index-vni/mobile-white-paper-c11-520862.pdf, Feb. 2017.

[3] M. R. Akdeniz, Y. Liu, M. K. Samimi, S. Sun, S. Rangan, T. S. Rappaport, and E. Erkip, "Millimeter wave channel modeling and cellular capacity evaluation," *IEEE Journal on Selected Areas in Communications*, vol. 32, no. 6, pp. 1164–1179, Jun. 2014.

[4] M. N. Tehrani, M. Uysal, and H. Yanikomeroglu, "Device-to-device communication in 5G cellular networks: challenges, solutions, and future directions," *IEEE Communications Magazine*, vol. 52, no. 5, pp. 86–92, May 2014.

[5] X. Lin, J. G. Andrews, and A. Ghosh, "Spectrum sharing for device-to-device communication in cellular networks," *IEEE Transactions on Wireless Communications*, vol. 13, no. 12, pp. 6727–6740, Dec. 2014.

[6] A. H. Sakr and E. Hossain, "Cognitive and energy harvesting-based D2D communication in cellular networks: Stochastic geometry modeling and analysis," *IEEE Transactions on Communications*, vol. 63, no. 5, pp. 1867–1880, May 2015.

[7] M. Afshang, H. S. Dhillon, and P. H. J. Chong, "Modeling and performance analysis of clustered device-to-device networks," *IEEE Transactions on Wireless Communications*, vol. 15, no. 7, pp. 4957–4972, Jul. 2016.

[8] J. G. Andrews, T. Bai, M. N. Kulkarni, A. Alkhateeb, A. K. Gupta, and R. W. Heath, "Modeling and analyzing millimeter wave cellular systems," *IEEE Transactions on Communications*, vol. 65, no. 1, pp. 403–430, Jan. 2017.

[9] K. Venugopal, M. C. Valenti, and R. W. Heath, "Device-to-device millimeter wave communications: Interference, coverage, rate, and finite topologies," *IEEE Transactions on Wireless Communications*, vol. 15, no. 9, pp. 6175–6188, Sept. 2016.

[10] T. Bai and R. W. Heath, "Coverage and rate analysis for millimeter-wave cellular networks," *IEEE Transactions on Wireless Communications*, vol. 14, no. 2, pp. 1100–1114, Feb. 2015.

[11] M. D. Renzo, "Stochastic geometry modeling and analysis of multi-tier millimeter wave cellular networks," *IEEE Transactions on Wireless Communications*, vol. 14, no. 9, pp. 5038–5057, Sept. 2015.

[12] A. Thornburg, T. Bai, and R. W. Heath, "Performance analysis of outdoor mmwave ad hoc networks," *IEEE Transactions on Signal Processing*, vol. 64, no. 15, pp. 4065–4079, Aug. 2016.

[13] X. Yu, J. Zhang, M. Haenggi, and K. B. Letaief, "Coverage analysis for millimeter wave networks: The impact of directional antenna arrays," *IEEE Journal on Selected Areas in Communications*, vol. 35, no. 7, pp. 1498–1512, Jul. 2017.

[14] Y. L. Ban, C. Li, C. Y. D. Sim, G. Wu, and K. L. Wong, "4G/5G multiple antennas for future multi-mode smartphone applications," *IEEE Access*, vol. 4, pp. 2981–2988, Jul. 2016.

[15] M. D. Renzo, W. Lu, and P. Guan, "The intensity matching approach: A tractable stochastic geometry approximation to system-level analysis of cellular networks," *IEEE Transactions on Wireless Communications*, vol. 15, no. 9, pp. 5963–5983, Sept. 2016.

[16] N. Deng and M. Haenggi, "A fine-grained analysis of millimeter-wave device-to-device networks," *IEEE Transactions on Communications*, vol. 65, no. 11, pp. 4940–4954, Nov. 2017.

[17] M. Haenggi, "The mean interference-to-signal ratio and its key role in cellular and amorphous networks," *IEEE Wireless Communications Letters*, vol. 3, no. 6, pp. 597–600, Dec. 2014.

[18] S. Singh, M. N. Kulkarni, A. Ghosh, and J. G. Andrews, "Tractable model for rate in self-backhauled millimeter wave cellular networks," *IEEE Journal on Selected Areas in Communications*, vol. 33, no. 10, pp. 2196–2211, Oct. 2015.

[19] M. Haenggi, *Stochastic geometry for wireless networks*. Cambridge University Press, 2012.

[20] C. A. Balanis, *Antenna Theory: Analysis and Design*. Hoboken, NJ, USA: John Wiley & Sons, 2005.

[21] T. S. Rappaport, G. R. MacCartney, M. K. Samimi, and S. Sun, "Wideband millimeter-wave propagation measurements and channel models for future wireless communication system design," *IEEE Transactions on Communications*, vol. 63, no. 9, pp. 3029–3056, Sept. 2015.
[22] M. Haenggi and R. K. Ganti, "Interference in large wireless networks," *Foundations and Trends in Networking*, vol. 3, no. 2, pp. 127–248, 2009.
[23] N. Deng, W. Zhou, and M. Haenggi, "The Ginibre point process as a model for wireless networks with repulsion," *IEEE Transactions on Wireless Communications*, vol. 14, no. 1, pp. 107–121, Jan. 2015.
[24] H. Elkotby and M. Vu, "Interference modeling for cellular networks under beamforming transmission," *IEEE Transactions on Wireless Communications*, vol. 16, no. 8, pp. 5201–5217, Aug. 2017.
[25] M. Haenggi, "The meta distribution of the SIR in Poisson bipolar and cellular networks," *IEEE Transactions on Wireless Communications*, vol. 15, no. 4, pp. 2577–2589, Apr. 2016.
[26] H. Alzer, "On some inequalities for the incomplete gamma function," *Mathematics of Computation*, vol. 66, no. 66, pp. 771–778, 1997.

PLACE PHOTO HERE

Na Deng (S'12-M'17) received the Ph.D. and B.S. degrees in electronic engineering from the University of Science and Technology of China (USTC), Hefei, China, in 2015 and 2010, respectively. From 2013 to 2014, she was a Visiting Student in Prof. Martin Haenggi's Group at the University of Notre Dame, Notre Dame, IN, USA. From June 2015 to November 2016, she was a Senior Engineer at Huawei Technologies Co., Ltd., Shanghai, China. Since then, she has been a lecturer with the School of Information and Communication Engineering, Dalian University of Technology, Dalian, China. Her scientific interests include networking and wireless communications, green communications, and network design based on wireless big data.

PLACE PHOTO HERE

Martin Haenggi (S'95-M'99-SM'04-F'14) received the Dipl.-Ing. (M.Sc.) and Dr.sc.techn. (Ph.D.) degrees in electrical engineering from the Swiss Federal Institute of Technology in Zurich (ETH) in 1995 and 1999, respectively. Currently he is the Freimann Professor of Electrical Engineering and a Concurrent Professor of Applied and Computational Mathematics and Statistics at the University of Notre Dame, Indiana, USA. In 2007-2008, he was a visiting professor at the University of California at San Diego, and in 2014-2015 he was an Invited Professor at EPFL, Switzerland. He is a co-author of the monograph "Interference in Large Wireless Networks" (NOW Publishers, 2009) and "Stochastic Geometry Analysis of Cellular Networks" (Cambridge University Press, 2018) and the author of the textbook "Stochastic Geometry for Wireless Networks" (Cambridge, 2012), and he published 14 single-author journal articles. His scientific interests lie in networking and wireless communications, with an emphasis on cellular, amorphous, ad hoc (including D2D and M2M), cognitive, and vehicular networks. He served as an Associate Editor of the Elsevier Journal of Ad Hoc Networks, the IEEE Transactions on Mobile Computing (TMC), the ACM Transactions on Sensor Networks, as a Guest Editor for the IEEE Journal on Selected Areas in Communications, the IEEE Transactions on Vehicular Technology, and the EURASIP Journal on Wireless Communications and Networking, as a Steering Committee member of the TMC, and as the Chair of the Executive Editorial Committee of the IEEE Transactions on Wireless Communications (TWC). Currently he is the Editor-in-Chief of the TWC. He also served as a Distinguished Lecturer for the IEEE Circuits and Systems Society, as a TPC Co-chair of the Communication Theory Symposium of the 2012 IEEE International Conference on Communications (ICC'12), of the 2014 International Conference on Wireless Communications and Signal Processing (WCSP'14), and the 2016 International Symposium on Wireless Personal Multimedia Communications (WPMC'16). For both his M.Sc. and Ph.D. theses, he was awarded the ETH medal. He also received a CAREER award from the U.S. National Science Foundation in 2005 and three awards from the IEEE Communications Society, the 2010 Best Tutorial Paper award, the 2017 Stephen O. Rice Prize paper award, and the 2017 Best Survey paper award, and he is a 2017 Clarivate Analytics Highly Cited Researcher.

PLACE PHOTO HERE

Yi Sun (M'06) received the Ph.D. degree in optical engineering from the Dalian University of Technology, Dalian, China, in 2002. From 2006 to 2007, she visited Stanford University as a Senior Visiting Scholar. She is currently a Professor with the School of Information and Communication Engineering, Dalian University of Technology. Her research interests include cognitive radio networks, green communications, underwater communications and artificial intelligence.